

# Long Range X-Ray Imaging Utilizing Coded Aperture Techniques and Dynamic Reconstruction

by

**Tiffany Lee**

Submitted to the Department of Nuclear Science and Engineering  
in partial fulfillment of the requirements for the degree of  
Bachelor of Science

at the

**Massachusetts Institute of Technology**

June 2008

Copyright © 2008 Tiffany Lee. All rights reserved.

The author hereby grants to MIT permission to reproduce and distribute publicly paper and electronic  
copies of this thesis document in whole or in part.

Author: \_\_\_\_\_

Tiffany Lee

Department of Nuclear Science and Engineering

May 9, 2008

Certified by: \_\_\_\_\_

*May 8, 2008*

Richard C. Lanza

Senior Research Scientist

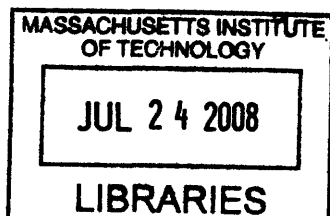
Thesis Supervisor

Accepted by: \_\_\_\_\_

David Cory

Professor of Nuclear Science and Engineering

Chairman, NSE Committee for Undergraduate Students



ARCHIVES

# **Long Range X-Ray Imaging Utilizing Coded Aperture Techniques and Dynamic Reconstruction**

by

**Tiffany Lee**

Submitted to the Department of Nuclear Science and Engineering on

May 9, 2008

In partial fulfillment of the requirements for the degree of  
Bachelor of Science in Nuclear Science and Engineering

## **Abstract**

Improvised explosive devices (IED) pose a very serious threat to civilians and military forces around the world, and new technologies must be developed for the early detection of these objects. Because of the high concentrations of low atomic number material such as nitrogen and hydrogen present in these explosives, x-ray backscattering provides a viable method of collecting information about these targets by analyzing their shape. Furthermore, a coded aperture used in conjunction with dynamic reconstruction algorithms offers high sensitivity and resolution even while the target is moving towards the detector. This paper describes a lab-based system that simulated a source-target-detector arrangement to be utilized in a radiation detecting vehicle in order to test dynamic reconstruction methods. Using a 225 kVp x-ray tube as the source, a medical CT-system camera fitted with a drill mask of 50% fill factor as the detector, and both radioisotope sources and low  $Z$  backscatter targets, images were acquired and reconstructed. The geometry of the experimental setup was optimized to reduce background noise from air scatter and environmental sources, as well as to prevent incident photons from directly reaching the detector from the x-ray tube. Measurements of a Co-60 point source and Co-57 area source with high activity generated high contrast images for which the shapes of the sources were clearly resolved. Acquisitions with varying target-detector distance of low  $Z$  materials, including a filled water jug and a four inch thick polyethylene arrow, produced lower contrast images in which the shapes were not as easily distinguished. The radioisotope tests were a proof of principle for dynamic reconstruction and the backscatter targets provided much insight on methods for improving the lab system, including the addition of steel behind the target, the narrowing of the detector energy window, and reassessment of the x-ray cone-beam.

Thesis supervisor: Richard C. Lanza

Title: Senior Research Scientist, Department of Nuclear Science and Engineering

## **Acknowledgements**

I would like to extend my sincere gratitude and appreciation to my thesis advisor Dr. Richard Lanza, who not only introduced me to the field of nuclear engineering, but also whose patience and guidance were instrumental to the completion of this thesis.

I would also like to acknowledge Jayna Bell, who sacrificed countless hours to help me in lab and provided direction for this thesis, Dr. Gordon Kohse, for all his insight in solving our problems, Dr. Berthold K.P. Horn, who carried the brunt of the research in programming, and other group members who worked behind the scenes at American Science & Engineering: Omar al-Kofahi, Christian Dinca, Joe Callerame, and Mike Winer.

I wish to thank my family and friends for providing unconditional and unending support throughout these four years. Nothing I say could begin to describe the depth of their love. Praise God for His grace in my life.

# Table of Contents

## 1. Introduction and Background

1.1 Explosives Detection Using Radiation.....	5
1.2 X-Ray Backscatter Imaging.....	7
1.3 Coded Aperture Techniques.....	11
1.4 Reconstruction Algorithms.....	13

## 2. Methods

2.1 Source, Target, and Detector Arrangement.....	16
2.1.1 Original Geometry Experimental Setup.....	17
2.1.2 New Geometry Experimental Setup.....	19
2.2 Calibration.....	21
2.2.1 Pulse Height Spectra.....	21
2.2.2 Steel Background Count Rates.....	25
2.3 Dynamic Reconstruction.....	29

## 3. Results and Discussion

3.1 Radioisotope Tests.....	31
3.1.1 Co-60 Point Source.....	32
3.1.2 Co-57 Area Source.....	34
3.2 Backscatter Targets.....	38
3.2.1 Original Geometry, Water Jug.....	39
3.2.2 New Geometry, Water Jug.....	41
3.2.3 New Geometry, Arrow.....	43

## 4. Conclusion.....

	46
--	----

## Appendix A: Background Isotopes.....

	49
--	----

## 5. References.....

	50
--	----

# **1. Introduction and Background**

## **1.1 Explosives Detection Using Radiation**

One of the most dangerous weapons used by insurgents around the world today is known as the improvised explosive device, or IED. So far, U.S. military sources have recorded more than 80,000 attacks in Iraq, such that these devices are now responsible for more than two-thirds of U.S. combat deaths in Iraq and an even higher percentage of wounds [1]. The rise of these types of explosives marks a turn in the type of warfare utilized, especially in Iraq and Afghanistan, and increases the need for research in the area of early explosives detection. Studies in this area extend into applications such as finding explosives in luggage, freight, and mail, landmine detection, and contamination monitoring. Methods for uncovering dangerous materials include particle, biochemical, and radiation detectors [2] and ongoing research strives to create new technologies with high sensitivity and success rate with low positive false alarm rates.

There are a number of detection methods utilizing x-ray radiation, including computed tomography (CT) systems, dual-energy analysis, and x-ray backscattering. The ability of x-ray imaging to differentiate material densities is particularly useful in for finding concealed chemical explosives for which the primary elements have very low atomic densities: hydrogen, carbon, nitrogen, and oxygen [3]. However, the mass densities of the elements are relatively high; explosives especially tend to have an unusually high presence of nitrogen. Some typical explosive components and their mass and low-Z element densities are listed in Table 1. Being able to differentiate harmful

from innocuous materials based on density is particularly important given that pliable plastic explosives can be molded into easily concealable shapes.

Material	Density (kg/m <sup>3</sup> )				
	Mass	Hydrogen	Carbon	Nitrogen	Oxygen
Ammonium nitrate	1700	85	0	595	1020
Nitroglycerine	1600	35	254	296	1015
PETN	1800	45	342	319	1094
TNT	1700	37	629	315	719
RDX	1830	49	297	693	791
HMX	1900	51	308	719	822
Black powder	1800	0	281	190	610
C4 (RDX-based)	1640	44	266	620	710
Smokeless powder	1660	39	402	325	984

*Table 1. Mass and element density of typical explosive materials [3]*

This investigation is part of a group project consisting of members of the MIT Nuclear Science and Engineering Department, the MIT Computer Science and Artificial Intelligence Laboratory, and American Science & Engineering, to build a lab-based test system for the testing of dynamic reconstruction algorithms for coded aperture imaging. The ultimate goal of the design is to be able to detect partially concealed explosive devices by use of x-ray backscattering using a moving detector. That is, the imaging system mounted on a vehicle could be able to accurately detect a hidden roadside bomb attached to a steel guardrail even while the vehicle is moving. In order to achieve this goal, the coded aperture system will be tested for its ability to image a target that moves towards the detector.

One particular reason why dynamic reconstruction is necessary for real-time explosives detection is the short amount of time available. The equations balancing the kinetic energy of the detecting vehicle with the energy to stop the vehicle can be written as Equation 1:

$$F \times x_{stopping} = \frac{1}{2} m v_0^2, \quad (\text{Eq.1})$$

where  $x_{stopping}$  is the stopping distance,  $m$  is the mass of the vehicle,  $v_0$  is its velocity,  $F$  is the force of friction,

$$F = \mu \times m \times g, \quad (\text{Eq.2})$$

and solving for the stopping distance gives

$$x_{stopping} = \frac{v_0^2}{2\mu g} \quad (\text{Eq.3})$$

Assuming a friction coefficient of 1 and a velocity of 30 miles per hour (or about 12 meters per second), the stopping distance required is about 7 meters. Adding 7 meters to the stopping distance to account for operator reaction time and assuming a blast radius of 35 meters, the total distance required is about 49 meters. This distance, divided by the vehicle velocity of 12 meters per second, gives a necessary detection time of about 4 seconds. Thus, a fast and long-range detection method is necessary to identify an explosive before the vehicle reaches it.

## 1.2 X-Ray Backscatter Imaging

The three main parts of the imaging system are the radiation source, the coded aperture or mask, and the reconstruction algorithm. The radiation source provides the photon signal that will be backscattered from the target. Because of the distance required

between the imaging camera and the target, this source will have to emit high energy x-rays as opposed to alpha or beta radiation.

Given the typical x-ray energies used in imaging (within a few hundred keV), it is expected that the modes of interaction with the target are by photoelectric effect and Compton scattering. The photoelectric cross section can be approximated by the relationship in Equation 4:

$$\tau \approx 10 \frac{Z^{4.5}}{E^3} \text{ barns/atom}, \quad (\text{Eq.4})$$

where  $\tau$  is the microscopic cross section,  $Z$  is the atomic number of the interacting material, and  $E$  is the energy of the incoming photon in keV. The microscopic cross section for Compton scattering,  $\sigma$ , is given in Equation 5:

$$\sigma = 0.665 \times Z \text{ barns/atom} \quad (\text{Eq.5})$$

A comparison of these two cross sections reveals that for the low  $Z$  materials, one can expect the prevailing mode of interaction to be Compton scattering.

Additionally, x-rays scattering with atomic electrons undergo both coherent and incoherent interactions. With coherent scattering, the photons retain their original energy without any energy transfer. On the other hand, an incident photon interacting by incoherent scattering transfers some of its energy and momentum to the electron.

Equation 6 describes the differential coherent scatter cross section.

$$\frac{d_{\kappa} \sigma_{coh}}{d\Omega} = \frac{d_e \sigma_0}{d\Omega} F^2[x, \rho_e(r)], \quad (\text{Eq. 6})$$



given in the units  $m^2/(k*sr)$ . Here,  $d_e\sigma_0/d\Omega$  is the Thomson different cross section per free electron per steradian and  $F$  is the coherent form factor that takes into account the electron distribution within the target material. At lower photon energies, the coherent scattering process occurs more often than the incoherent process, and the distribution of scattering angles is strongly biased towards the forward direction [4]. The differential incoherent scatter cross section is given by Equation 7.

$$\frac{d_{\kappa}O_{inc}}{d\Omega} = \frac{d_e\sigma_0}{d\Omega} F_{KN} S(x, Z), \quad (\text{Eq.7})$$

again in units of  $m^2/(k*sr)$  and where  $F_{KN}$  is the Klein-Nishina factor describes the probability of interaction with a free electron and  $S$  takes into account the electron binding energy's effect on scattering probability.

Radioactive sources have potentially higher energy and more penetrating gamma rays, but also pose the important problem that they cannot be “turned off” or completely attenuated, so nearby workers are always exposed to some radiation dose. They are more dangerous to handle, but do not require any additional equipment to use besides shielding. In addition, if these sources are stolen, they can be used as a part of radiological weapons, thus posing a large security concern. On the other hand, x-ray tubes only provide photons when a large voltage is applied, so the x-ray tubes can be turned off when not in use. The primary concern for an x-ray tube is that its emitted energy increases as applied voltage increases, but this photon energy for most models levels off at higher voltages, thus introducing a maximum photon energy and a maximum backscattered energy.

An imaging system using x-ray technology has three primary benefits: The acquired signal is directly proportional to the density of the material being examined, the detector only needs access from a single side, and a high contrast image is obtainable [5]. The first benefit is particularly important because many explosive devices have specific chemical compositions including low-atomic number elements such as nitrogen and hydrogen [6]. Thus, x-ray backscattering allows the operator to identify explosives by finding unusually high concentrations of these low  $Z$  materials. The second benefit is also useful because a two-sided source-detector setup usually requires a very large detector, which can be expensive especially if large amounts of scintillator liquid are needed. A single-sided detector such as the one proposed in this design only requires a detector of about  $0.4 \times 0.4 \text{ m}^2$ . Finally, high contrast (or signal-to-noise ratio) and high resolution are always necessary in imaging systems to maintain a low false alarm rate. The signal-to-noise ratio,  $SNR$ , depends on the number of photons counted,  $n$ , as shown in Equation 8.

$$SNR \propto \sqrt{n} \quad (\text{Eq.8})$$

One of the most important quantities to determine for a system that utilizes x-ray backscattering techniques is the backscattering fraction, or the effective fraction of x-ray photons that scatter from the target and whose information can be retrieved for image reconstruction. Figure 1 below describes the average backscatter energies given source energies that are typical for x-ray tubes. The backscatter energy is clearly a fraction of the source energy, so it is necessary to optimize the system such that the system maintains maximum backscatter energy for a minimum source energy.

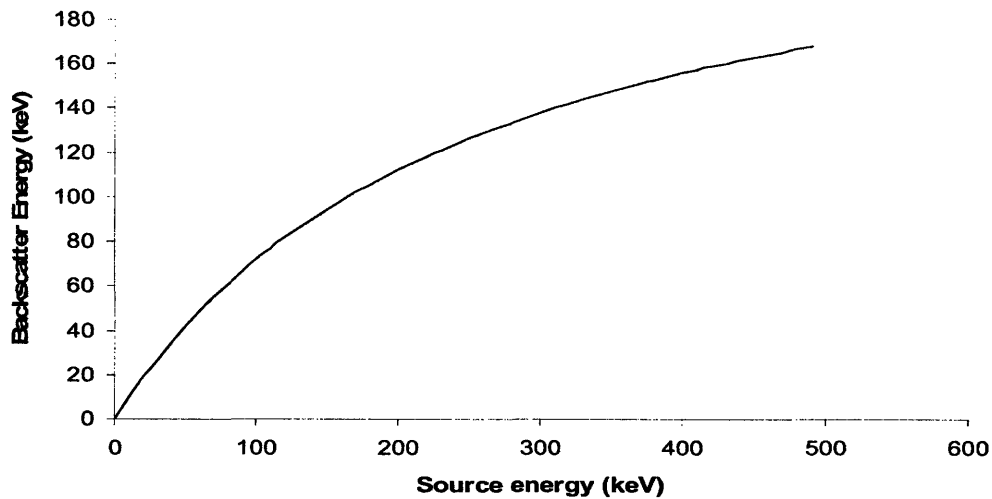


*Figure 1. Backscatter energy as a function of source energy for typical x-ray tube energies.*

Although this comparison of radioactive sources versus x-ray sources demonstrates the higher effectiveness of x-ray sources for this apparatus, both types of sources will be used to test the imaging system. As described below in the Methods section, utilizing radioactive sources in conjunction with the coded aperture system helps to establish a proof of principle for the dynamic reconstruction algorithms. The Co-60 point source and the Co-57 area source provide a much stronger signal than x-ray backscattering does, so that the effectiveness of the reconstruction can be determined even if there is significant background noise.

### **1.3 Coded Aperture Techniques**

The second major part of the apparatus is the coded aperture itself. The pinhole camera is a well-known technique for obtaining an image with increase resolution at the expense of limited sensitivity. One solution to this problem is the use of a multi-pinhole camera so that resolution is retained while increasing the amount of information from the

object reaching the detector, thus improving the signal-to-noise ratio. This method is referred to as the coded aperture technique. Different sizes and structures of masks are designed for different applications due to their specifications that allow for enhanced sensitivity or spatial resolution. The spatial resolution achieved through coded aperture collimation depends especially on the intrinsic resolution of the detector and the bore size of the holes in the mask. The primary difficulty with the coded aperture technique is the reconstruction algorithm, which is necessarily more complicated than that of a regular pinhole camera due to the different positions and orientations of photons entering the detector. The image produced from each hole overlaps slightly with those produced by nearby holes, and the reconstruction algorithm must correct for this superposition in order to create a coherent total picture [7]. Additionally, the different angles between each hole and the object must be accounted for.

A coded aperture is necessary because it protects the camera from overexposure and focuses the photons in order to increase the resolution of the detected image for a certain area of the camera. Multiple holes in the aperture provide more space for photons to pass through, and thus a higher amount of information to enter the camera and a higher signal-to-noise ratio. However, these holes must be spaced out such that it is possible to combine the information produced by each hole and retrieve a coherent total image. In other words, each pinhole forms a copy of the projection of the object, and the superposition created by multiple pinholes must be corrected or decoded according to the array of pinholes [8]. The additional empty space introduced by pinholes also lowers the weight of the coded aperture.

Moreover, the test design is used to test the reconstruction algorithms for the coded aperture. Given the spacing of the holes in the coded aperture, the reconstruction algorithm has to be able to retrieve a total image given the backscattered photons passing through each hole. In addition, the algorithm has to be able to image the target while it is moving towards the camera. The test design is also used to measure the amount of photons backscattering to the camera in order to verify whether the amount of information relayed back to the camera is enough to produce an accurate, high resolution, and high contrast image.

## **1.4 Dynamic Reconstruction**

The reconstruction of data acquired through a coded aperture typically requires two primary steps: the convolution and the deconvolution. One common aperture type is the modified uniformly redundant arrays (MURA), which makes the reconstruction process simpler because at any point on the mask, the detector sees the same number of holes. On the mask, a particular unit pattern produces a data set that can be interpreted with the appropriate deconvolution algorithm, and this unit pattern is tessellated through the mask at fixed orientations [9]. This method can be repeated for as large a mask as is necessary to achieve the desired field of view. Increasing the number of tessellations also decreases the fill ratio of the mask to increase the signal-to-noise ratio. An example of the MURA aperture type is shown in Figure 2.

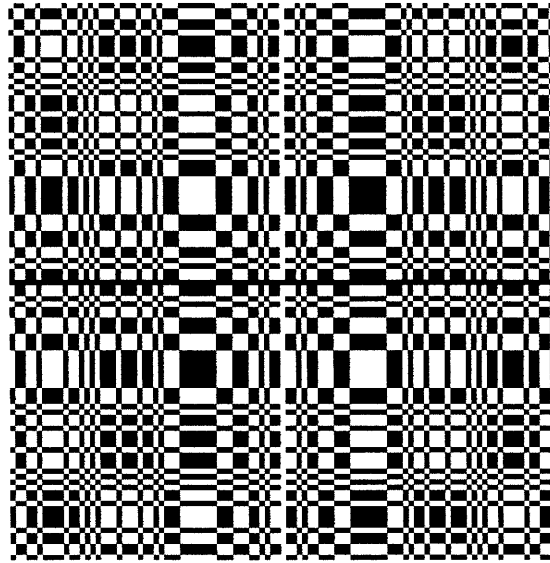


*Figure 2. An example of a 103 x 103 MURA.*

However, this study utilizes a hexagonal mask design as shown in Figure 3.

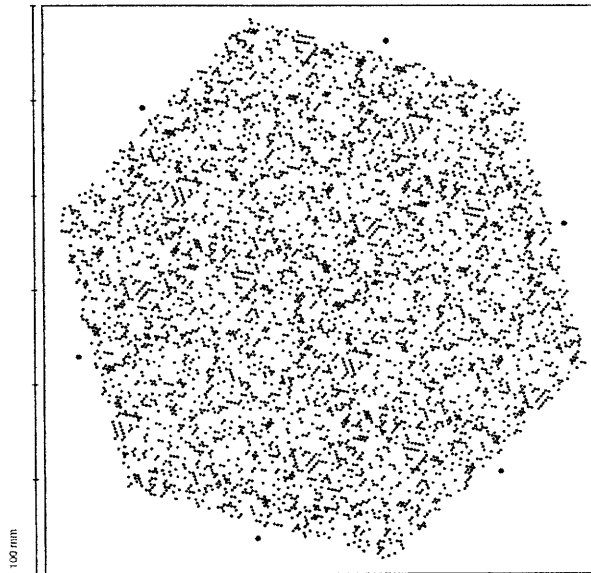


*Figure 3. Drill mask design with 25% fill factor.*

The dynamic reconstruction code for this investigation was written by Dr. Berthold K.P. Horn. It differs significantly from the typical coded aperture techniques because it resolves images using back projection rather than the convolution and discrete

Fourier transform. Essentially, each open hole and blocked portion of the mask corresponds to a voxel in a 3-D environment, and each event that passes through the collimating mask and into the detector is recorded at a certain spatial position within the 3-D area and weighted according to the hole's position on the mask. This is described graphically in Figure 4.

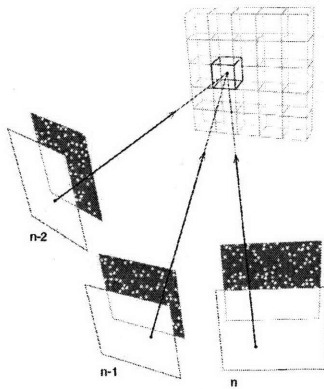


*Figure 4. Graphical representation of how events entering the mask are mapped to a particular voxel in a 3-D array.*

Subsequent events through the same hole continue to add value to that particular voxel, thus building up the pixel value according to the amount of signal. Also, a photons backscattered from one position on the target can scatter at different angles and enter the detector at different locations since the mask holes are not infinitely small, as shown in Figure 5.

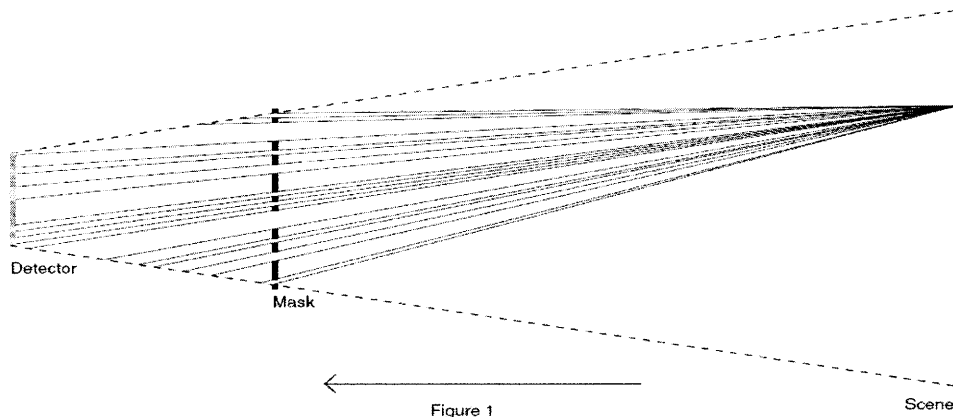


*Figure 5. Scattered events from the target pass through the mask at different angles and enter the detector.*

This method is important because of the relatively low amount of backscatter and therefore the low amount of signal that the detector receives. Additionally, this method makes it easier to use different mask designs or even multiple detectors.

## **2. Methods**

### **2.1 Source, Target, and Detector Arrangement**

The relative positions of the x-ray tube, the target, and the coded aperture simulate the real conditions of a source and detector mounted on a truck. Although the finished product of this project may utilize a much higher energy x-ray tube as its radiation source due to its increased amount of backscatter, other sources can be implemented in the test system for the proof of concept for both the coded aperture and dynamic reconstruction. The experiment includes three sources: a monoenergetic radioisotopic point source, a monoenergetic radioisotopic flood source, and an x-ray tube. Tests using the point source ensure that the energy windows for the Anger camera are set



to collect the gammas and backscattered x-rays. The flood source allows for the testing of shapes and how well the camera can distinguish them from background. Finally, the x-ray tube measurements examine the effects of the x-ray spectrum and the effects of the energy windows on the image.

### 2.1.1 Original Geometry Experimental Setup

The following initial measurements have been made for the experimental setup:

- Detector (Anger Camera)
  - Front square area: 0.38 x 0.38m
  - Resolution: 3mm at experimental energies
- Mask
  - Area: 0.31 x 0.31m
  - Field of view: 1.68 x 1.68 m<sup>2</sup>
- Geometry
  - Detector to mask distance: 0.6m
  - Mask to target distance: 5.0m
  - Magnification: 0.12
  - Image resolution: 25mm/pixel
  - X-ray cone beam illuminates 0.5 x 0.5m<sup>2</sup> of the field of view

Figure 6 displays the setup of the imaging systems given the above conditions.

The lab-based system has the same size detector and mask, but the distance between the mask and target (and thus the magnification and field of view), as well as the orientation of the x-ray cone-beam, are modified due to the space restraints of the lab setup.

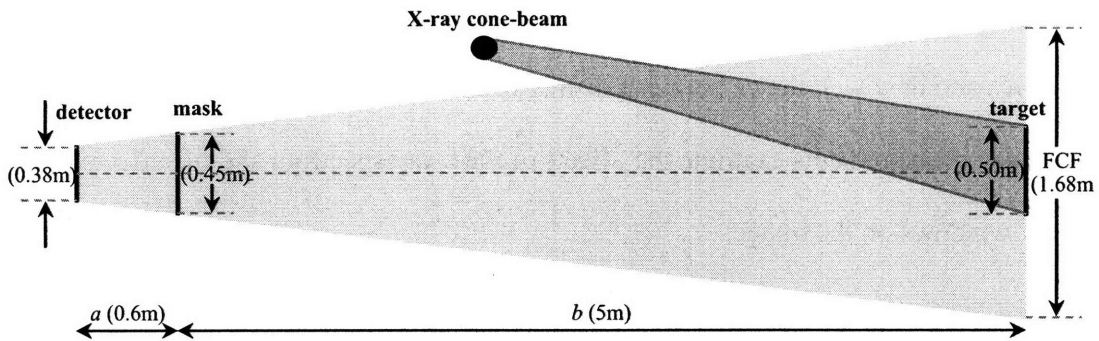
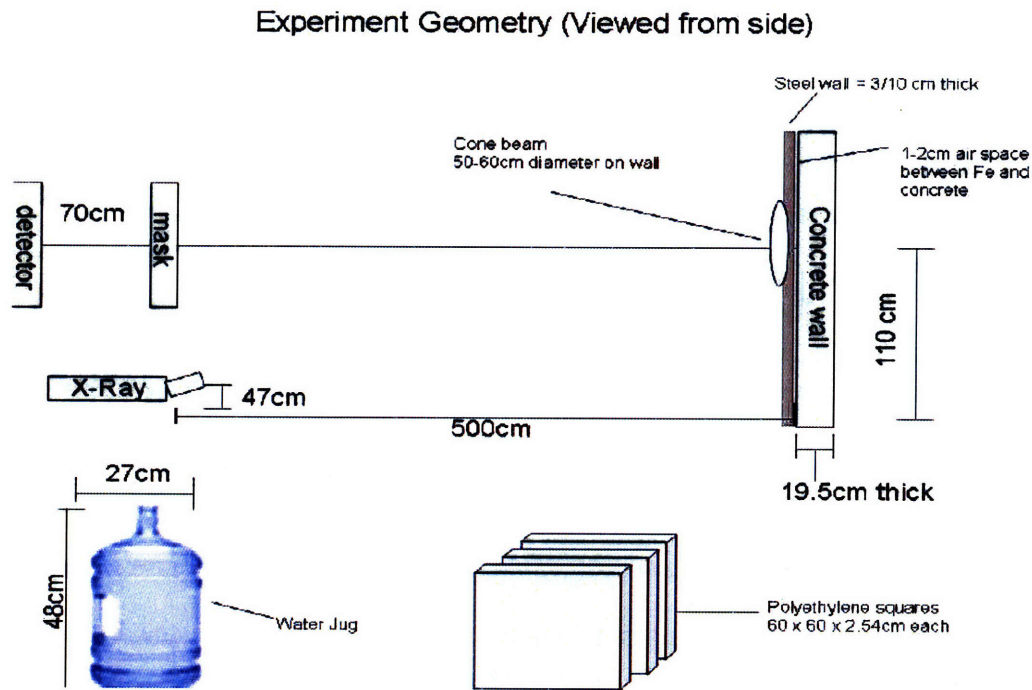


Figure 6. Coded aperture imaging system setup and geometry.

The most important points are to simulate a typical distance between the target and the detector (to be able to detect the IED before actually reaching it), and to maintain as small a detector as possible while maintaining a good-sized field of view and high resolution image.

Figure 7 depicts the original geometry for the experimental setup as well as some of the objects used for preliminary testing. The x-ray tube placed on the ground and tilted upwards produces a cone of x-ray signal that hits a concrete wall layered with steel in front. Low Z targets such as the water jug and polyethylene sheets placed in front of the steel reinforcement and within the cone-beam will backscatter a percentage of the x-rays back to the mask, and the signal passing through the mask reach the actual detector.



*Figure 7. Original experimental setup.*

The targets sit on a small table so that they enter the field of view of the detector. For measurements at different distances, the table and target are pulled forward using a small tug. The experiments of this study involve targets moving in the z-direction, and utilizing the mechanical tug helps maintain spatial invariance in from side to side in relation to the mask field of view.

### **2.1.2. New Geometry Experimental Setup**

After preliminary testing, proposed changes to the geometry of the experimental setup (shown in Figure 8) were made in order to improve image quality by reducing background noise.

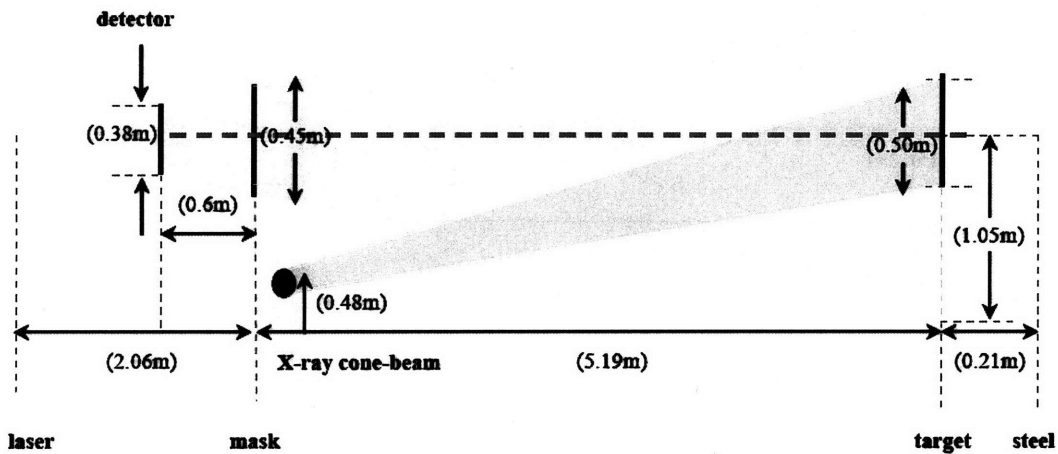


*Figure 8. New geometry of the experimental setup.*

There were three major changes; first of all, an increase was made in the distance between the mask and target achieved by moving the gantry of the x-ray CT system further left. The reason for this is because the point and area sources stored in the room are located close to the target area, and moving the detector away from those sources could decrease background noise from those sources.

The second change was a slight decrease in the distance between the x-ray source and the target achieved by moving the x-ray tube to the right. This allows for a larger amount of signal to scatter off the target, however, it also decreases the size and changes the position of the cone beam.

Finally, the addition of a lead shield placed vertically between the x-ray tube and the mask aids in reducing the amount of radiation leakage from the side of the x-ray source that reaches the detector, without obscuring the field of view of the mask. This extra shield is shown in Figure 9.

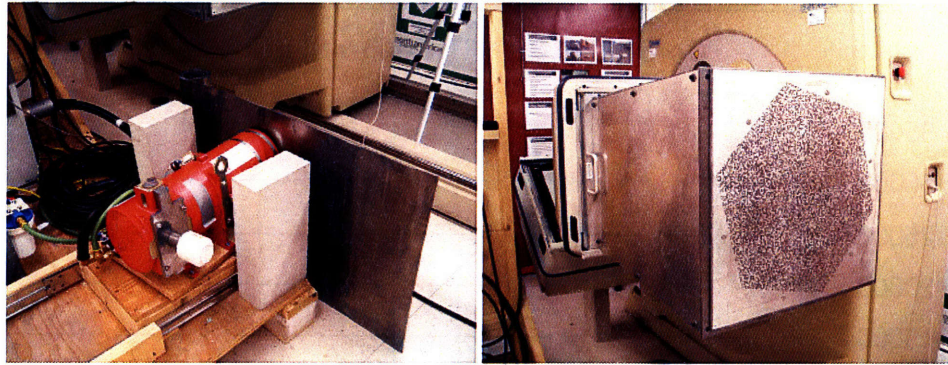


*Figure 9. 1) Lead shield between x-ray source and detector 2) Detector head with mask*

## **2.2 Calibration**

Two major preliminary tests were conducted regarding the energy spectrum received by the detector mask and the effects of steel background thickness on backscattered photon count rate. The purpose of these measurements was to help optimize the experimental setup and camera protocols to acquire images with higher SNR by reducing noise.

### **2.2.1 Pulse Height Spectra**

The pulse height spectra were obtained using a HPGe detector placed in front of the mask. First, a calibration curve was acquired using a Co-57 source and a Cs-137 source, which produce three peaks for calibration at 122.0 keV, 136.4 keV, and 661.6 keV.

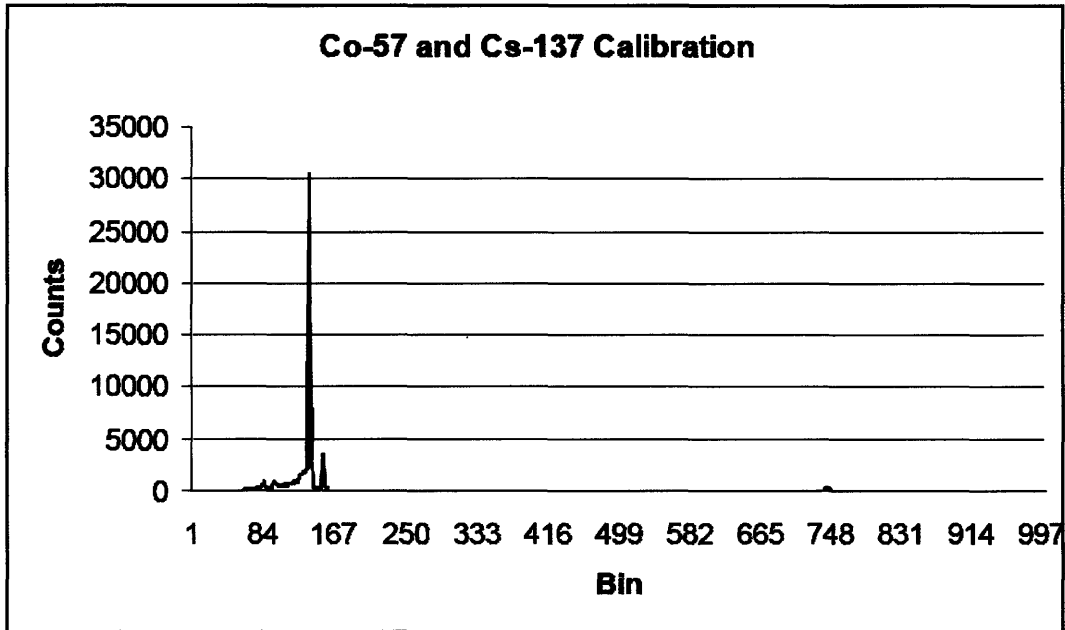


*Figure 10. Calibration curve acquired by HPGe.*

Calibrating according to those three peaks in Figure 10, pulse height spectra of the background was taken to ensure that there were not any additional radioisotopes near the laboratory setup that could produce additional radiation that would interfere with the target's scattered photons. Pulse height spectra were also taken while the x-ray was on with only a steel background and with polyethylene sheets, recorded in Figure 11.

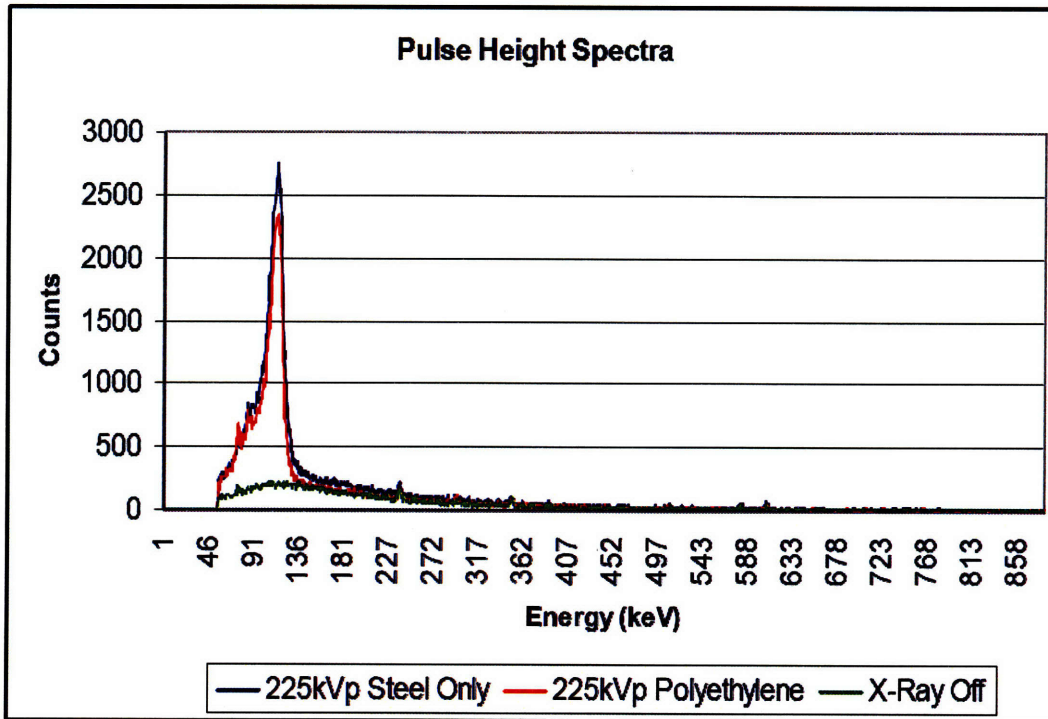


Figure 11. Comparison of pulse height energy while the x-ray is on and off.

The pulse height spectra with the x-ray on have their peaks centered such that the open energy window of 85 – 140 keV thoroughly encompasses the entire peak, which is expected from the 225 kVp x-ray tube. Using an open energy window ensures that the detector receives the maximum amount of signal; however, it also carries the risk of introducing more noise including background sources and air scatter. Moreover, the comparison of the peaks generated by the x-ray measurement with steel only and with polyethylene reveals that the presence of a polyethylene target does not significantly change the energy spectrum detected by the Anger camera.

One of the primary concerns was a small peak that indicated the presence of radioactive Pb-214 with half-life 26.8 minutes that could stem from activated lead used in the laboratory. To test this, the pulse height spectra was recorded a second time after a period of 30 minutes (corresponding with the half-life of Pb-214). This is shown in Figures 12 and 13:

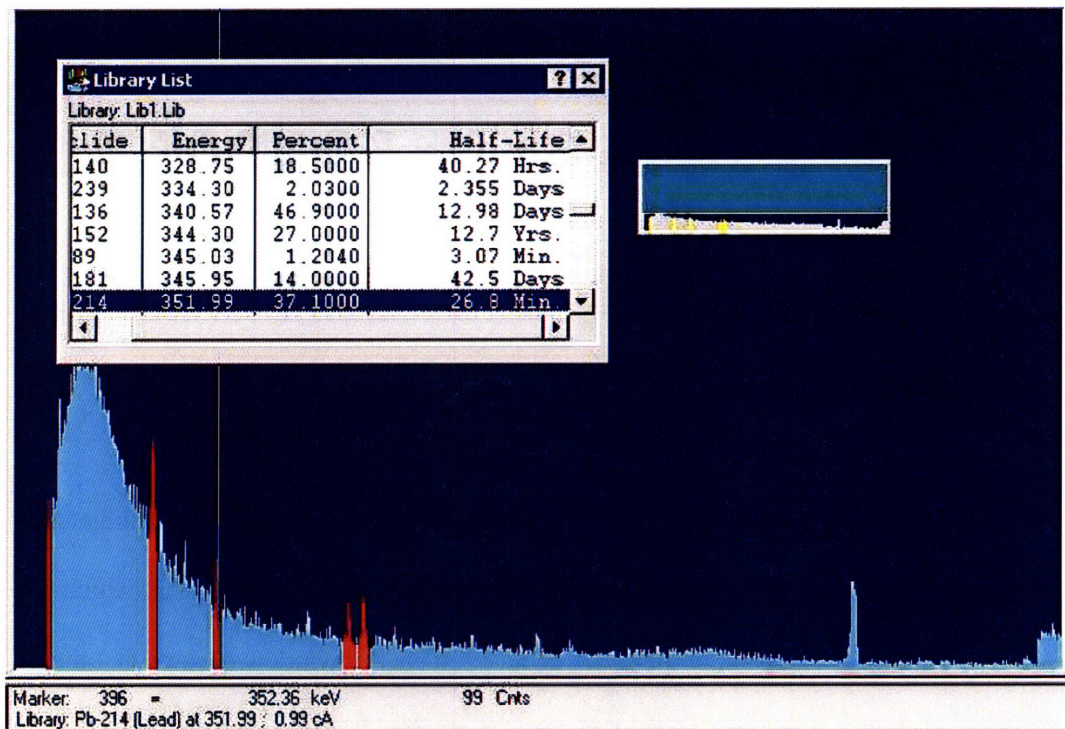


Figure 12. Pulse height spectra of the background with x-ray off. Energy peak for Pb-214 is highlighted.



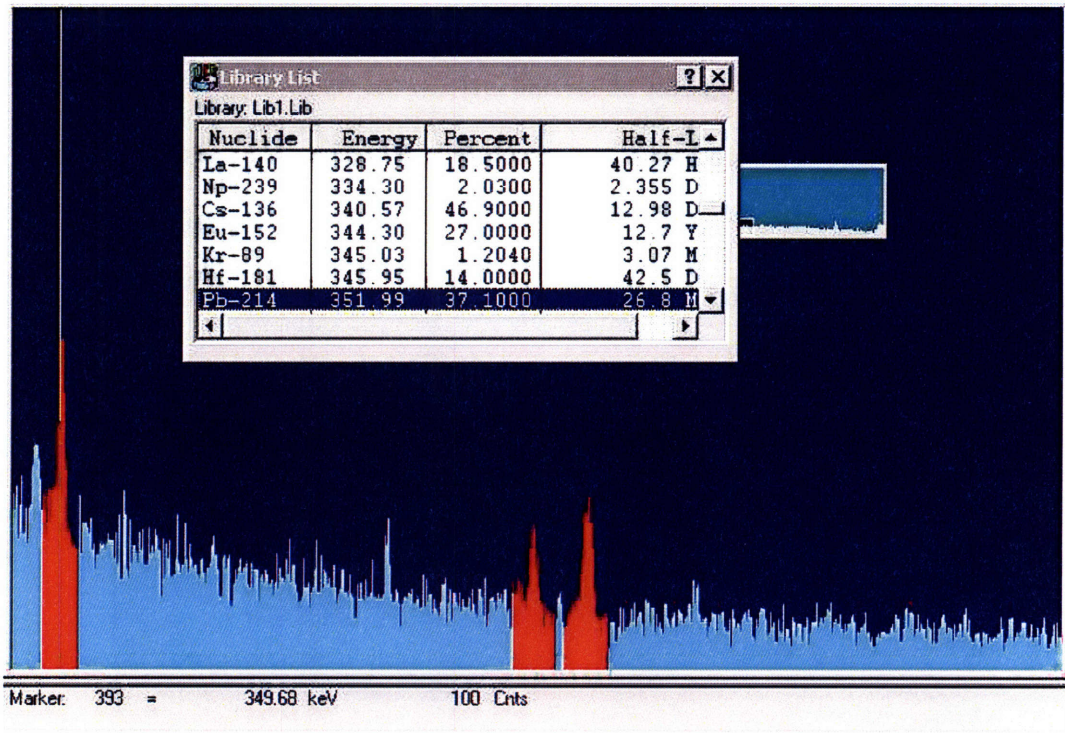


Figure 13. Pulse height spectra taken 30 minutes after that of Figure 12.

The second measurement revealed almost the same number of counts for Pb-214 as the first measurement did, 100 counts as opposed to 99 counts in the first measurement, given approximately the same acquisition time. Because of the similar count rates, it is expected that there is not a significant generation of Pb-214 that could distort the acquisitions. Beyond Pb-214, some of the other isotopes found included small amounts of Ba-131 and Xe-135. A full list of the isotopes is found in Appendix A.

## 2.2.2 Background Steel Count Rates

One of the purposes of this study is to simulate a real-life scenario involving a roadside bomb. For this scenario, it is expected that the explosive would be attached to a steel guardrail about two centimeters thick. In order to simulate this condition, layers of

steel are placed behind the target. Increasing the thickness of the steel background can decrease the background noise of the image and increase the signal to noise ratio since the steel is better able to absorb x-rays that do not backscatter from the target. This is because steel has a higher density and atomic number than the lower Z materials of the target and concrete background. To test this, the count rates were recorded through the different thicknesses of steel and the images should reflect an increased brightness with each additional layer. The three layers of steel are shown in Figure 14. Figures 15 and Table 2 display the count rates as a function of steel thickness.

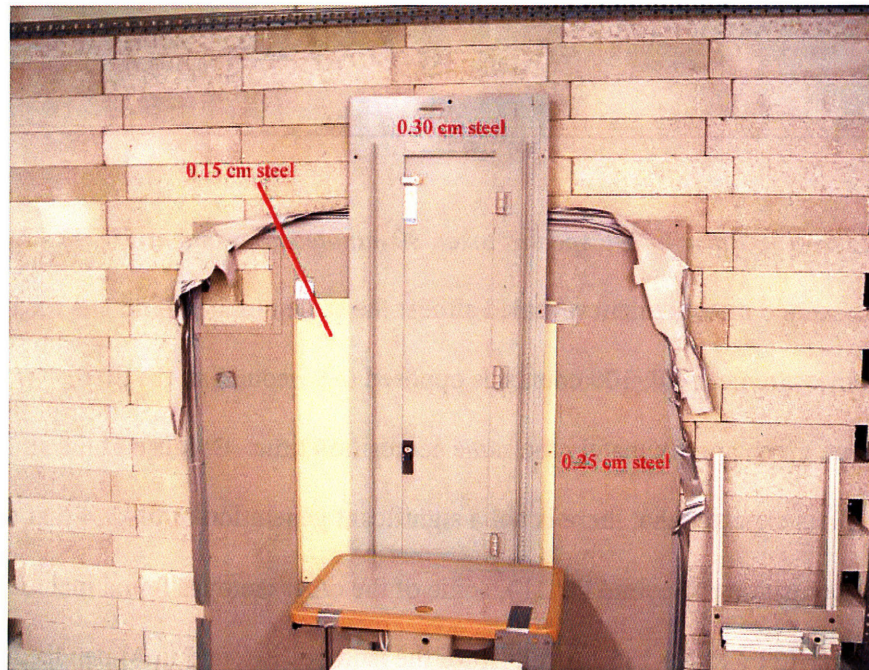


*Figure 14. The three layers of steel background on concrete.*

<b>X-ray voltage</b>	<b>225 kVp</b>	
<b>X-ray current</b>	<b>13.3 mA</b>	
<b>Energy window</b>	<b>85 – 140 keV</b>	
<b>Background count rate</b>	<b>~900 cps</b>	
<b>Total counts</b>	<b>100k</b>	
<b>Acquisition</b>	<b>Distance (cm)</b>	<b>Count rate (cps)</b>
<b>Background, no x-rays</b>	<b>522.5</b>	<b>65</b>
<b>Background x-rays on concrete only</b>	<b>522.5</b>	<b>2300</b>
<b>Steel, 0.25 cm</b>	<b>522.25</b>	<b>1850</b>
<b>Steel, 0.40 cm</b>	<b>522.1</b>	<b>1700</b>
<b>Steel, 0.70 cm</b>	<b>521.7</b>	<b>1450</b>
<b>Steel, 0.70 cm + arrow target</b>	<b>465.8</b>	<b>2000</b>

*Table 2. Specifications for the x-ray tube and detector and count rate recorded against steel thickness.*

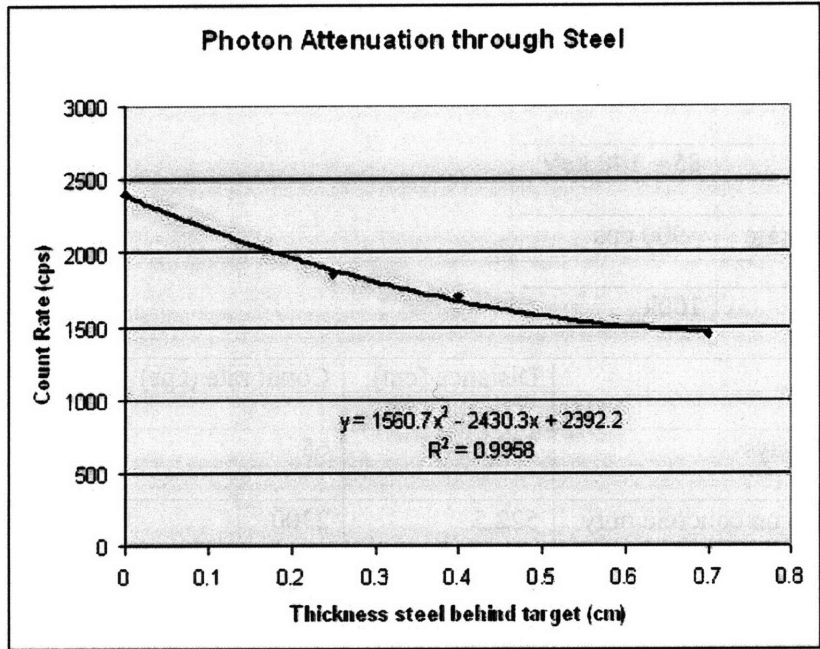
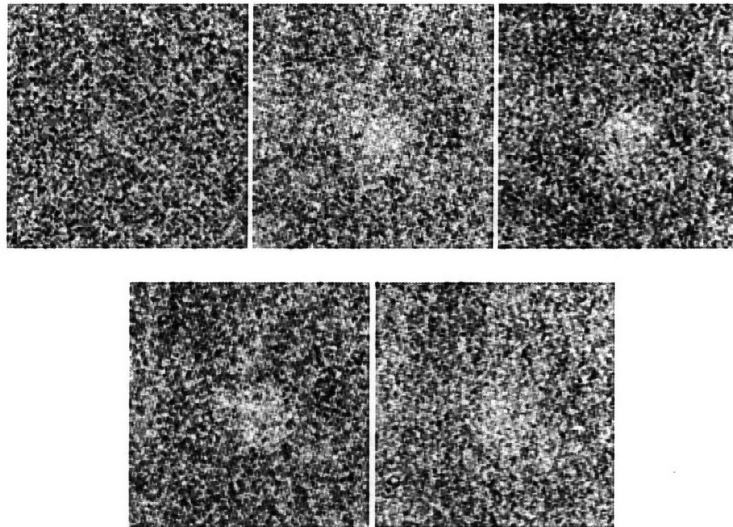


Figure 15. Photon backscatter count rate as a function of steel thickness.

Figure 15 clearly demonstrates the utility of the steel background in reducing x-ray backscatter. Thus having the steel background improves image quality of the target by reducing backscatter from behind the target.

In Figure 16, the sequence of images without a target show a bright zone in the center where the x-ray cone-beam reflects off the steel background. As the layers of steel are added, the change in the brightness of the images is apparent.



*Figure 16. The brightness of the image differs depending on the thickness of the steel background; 1) concrete only 2) 0.25 cm steel 3) 0.40 cm steel 4) 0.70 cm steel 5) 0.70 cm steel and a polyethylene target*

## **2.3 Dynamic Reconstruction**

The dynamic reconstruction algorithms use concepts similar to back projection. When a photon passes through one of the holes in the mask and hits the detector, it is possible to determine the position in the actual scene where the photon originated from, given that the mask position and orientation are known. In this case, each event is stored in a 3-D voxel array that accumulated value as the event is detected at a certain cell on the camera face. Figure 17 describes how two incoming signals generate counts on the detector depending on how much of the signal passes through the holes in the mask. The number of counts is then added in the array.

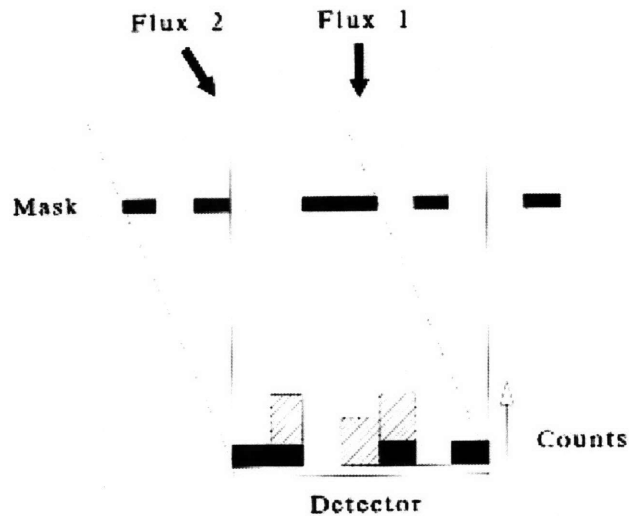


*Figure 17. Graphical representation of the accumulation of counts in each voxel depending on the mask orientation. [10]*

What makes the reconstruction algorithms used to generate images in this study dynamic is simply that the voxel array is updated for each event recorded. However, the detected events do not simply add the same value to each corresponding voxel because this would cause counts to accumulate everywhere. In order to help suppress the excess noise, and also because the typical mask does not have exactly equal open and closed areas, the voxel count is increased depending on the amount of closed area on the mask and is decreased depending on the open area on the mask. Additional weights that affect the value added or subtracted from a voxel include the orientation of the photon relative to the axis of the detector and mask and the distance between the hole and the detector element.

The hexagonal mask design used in this study is shown in Figure 18.

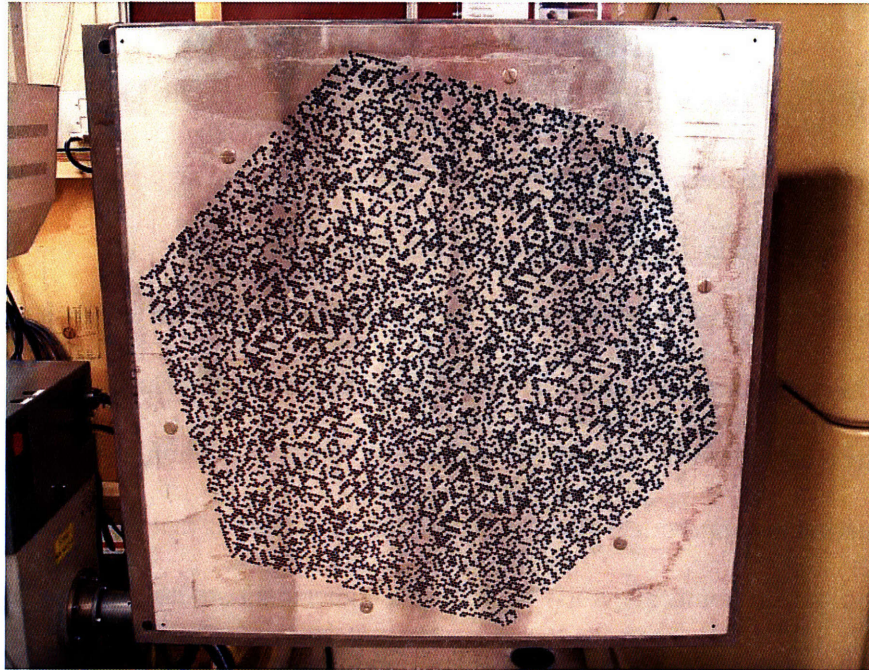


*Figure 18. Hexagonal mask, 50% fill factor.*

Mask specifications:

- Material: Pb-Sb
- Anti mask with  $60^\circ$  rotation
- Fill factor: 50%
  - 21421 elements, 10711 open, 10710 closed
- Thickness: 3.1 mm
- Space between holes: 3.5 mm
- Size: 600 mm x 600 mm; drill pattern tilted  $15^\circ$  to fit the largest hexagon

### **3. Results and Discussion**

#### **3.1 Radioisotope Tests**

Even though the final system is designed to accommodate an x-ray source, testing radioisotopes still help prove the principles of coded aperture imaging. The higher count rates obtained from radioisotopes produce increased contrast in the reconstructed images and results show that the shapes of the sources can be resolved.

### **3.1.1 Co-60 Point Source**

In order to make sure that the Anger cameras are functioning properly, they should be tested by imaging gamma-radiation emitting sources. These monoenergetic radioisotopes produce point source images with a higher photon count rate than scattering targets. The point source can easily be moved around to prove the principles for the dynamic reconstruction algorithms as a preliminary study. In addition, these tests will help in determining appropriate energy windows for the detectors that will cancel out background and environmental noise to produce a higher signal-to-noise ratio. The reconstructed images from this test are displayed in Figure 19.

Co-60 Point Source specifications:

- Active area: 1 mm diameter
- Thickness: 3.2 mm
- Reference date: December 1, 2007
- Initial activity: 345  $\mu$ Ci

The point source is placed inside a lead tube with its opening pointing towards the detector. Thus the expected image of the Co-60 point source is a small bright spot with a diameter comparable to the diameter of the lead tube.



X-ray voltage	225 kVp	
X-ray current	13.3 mA	
Energy window	85 – 140 keV	
Background count rate	~900 cps	
Total counts	100k	
Acquisition	Distance (cm)	Count rate (cps)
Co-57 point source, center	518.5	1250
Co-57 point source, 20 cm right	518.5	1200
Co-57 point source, 20 cm above	518.5	1250

*Table 3. Specifications for the x-ray tube and detector with count rates for the Co-57 point source.*

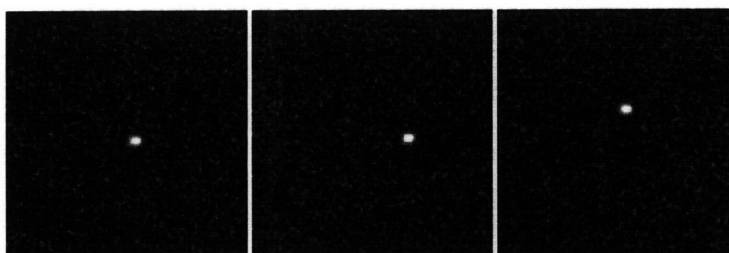


*Figure 19. Co-60 point source in the 1) center 2) 20 cm right and 3) 20 cm above orientations*

The images shown in Figure 19 reveal a very strong contrast between the source and the background. Even as the source position changes between the center arrangement and 20 cm right and above arrangements, the spot contrast is still very high. These results also show ensure that the detector field of view will include the x-ray cone beam, which is centered around the initial position of the point source and whose radius extends approximately 25 cm in each direction.

### 3.1.2 Co-57 Area Source Test

The purpose of area source tests is to determine whether radioisotope shapes are distinguishable. This test utilizes a rectangular Co-57 area source partially obscured by a lead cutout (Figure 20) that produces shapes distinguishable in the reconstructed images. The lead cutout also aids in reducing the count rate, which is already much higher than the count rates expected from x-ray backscatter.

The Co-57 flood source specifications:

- Area: 638 x 454 mm diameter
- Active area: 610 x 419 mm diameter
- Reference date: December 13, 2007
- Initial activity: 5 mCi
- Half-life: 271.77 days
- Energies: 122 keV (85%), 136 keV (10.6%), 14.412 keV (9.5%)

Lead cutout dimensions:

- Total height: 33 cm
- Height of cutout section: 24 cm
- Thickness: 0.6 cm

For this experiment, the lead cutout and area source are propped up in between lead bricks on the target's stand and pulled forward using the tug. A higher number of total counts was used due to the very high count rate of the area source, which remained at a high level of activity. The initial energy window for the first part of this measurement centered around the most abundant energy of Co-57, 122 keV, and varied by +/- 10%. The z-distance varied by approximately six cm per acquisition for the first six acquisitions.



Figure 20. Lead cutout placed in front of the area source.

X-ray voltage	225 kVp	
X-ray current	13.3 mA	
Energy window	116 – 128 keV	
Background count rate	~900 cps	
Total counts	2000k	
Acquisition	Distance (cm)	Count rate (cps)
Area Source	537.0	6700
Area Source	530.8	7200
Area Source	524.9	7200
Area Source	518.7	7400
Area Source	512.1	7500
Area Source	505.5	7600

Table 4. Specifications and count rates for the first six acquisitions of the Co-57 area source.

Following the first six acquisitions, the energy window was slightly widened to 122 keV +/- 20% in order to see whether there would be a significant increase in count rate.

X-ray voltage	225 kVp	
X-ray current	13.3 mA	
Energy window	110 - 134 keV	
Background count rate	~900 cps	
Total counts	2000k	
Acquisition	Distance (cm)	Count rate (cps)
Area Source	499.1	11000
Area Source	492.7	11000
Area Source	486.2	12000
Area Source	479.4	12000
Area Source	472.5	12000
Area Source	466.5	12000
Area Source	460.8	13000
Area Source	440.7	13000
Area Source	421.0	14000

*Table 5. Specifications and count rates for the Co-57 area source at a wider energy window.*

The larger energy window produced a much higher count rate for the area source ranging from about 4000-6000 counts per second more. This was in addition to the higher count rate due to the smaller distance in between the detector and target. Most likely, the primary reason for the increased count rate is the inclusion of the 136 keV

photons emitted from Co-57. Additionally, photons undergoing air scatter and arriving at the detector at energies lower than 122 keV or 136 keV would also be included in the higher count rate.

The set of reconstructed images recorded over varying distances between the mask and area source target show that the unobscured parts of the area source are clearly resolved in the images, shown in Figure 21.

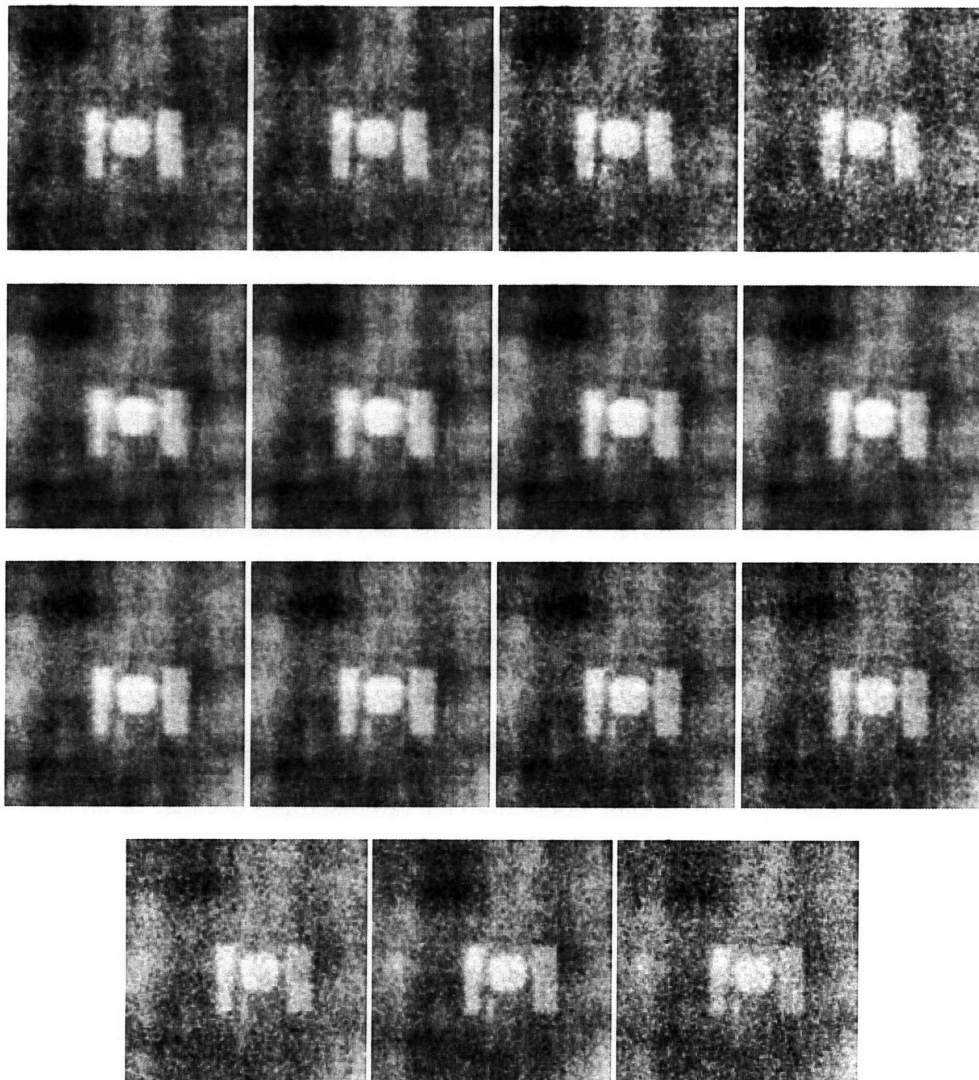


*Figure 21. Sequence of fifteen acquisitions of the Co-57 area source, starting from the furthest distance (537 cm) to the closest (421 cm).*

In these images, even the slight gap in between the lead bricks that propped up the lead cutout in front of the area source could be resolved. The contrast between the source and background is clearly not as strong as that of the point source tests, and some of the images have significant noise. Upon careful examination of these reconstructed images, it is also shown that there is a slight spatial variance of the target from left to right. This could indicate a minor problem with the use of the tug in the experimental setup that is causing the target to meander left and right instead of moving only in the z-direction. Still, the clear semi-circular shape of the center of the lead cutout proves that the principles of dynamic reconstruction work even with varying z-distances.

### **3.2 Backscatter Targets**

The low Z materials in the backscatter targets simulate the materials expected in explosive devices. Even though the backscattered photon energies do not sufficiently vary enough for the system to differentiate materials, there is much utility in the low Z elements for their high probability of backscatter. These targets help in understanding whether the coded aperture system is capable of resolving rounded edges, such as those of the water jug target, or sharp edges, as in those of the arrow target. In both cases, the targets produce a much smaller photon count than the radioisotopes because of the high activity of the isotopes and the lower probability of close to 180-degree backscatter.

### 3.2.1 Original Geometry, Water Jug Target

Initial tests using the original geometry shown in Figure 7 above using the filled water jug target were conducted by Jayna Bell. Figure 22 displays the reconstructed image taken at 1000k counts.

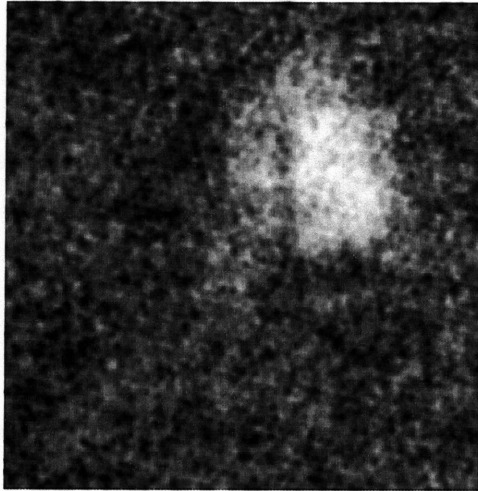


*Figure 22. Reconstructed image of the water jug target.*

The reconstruction revealed a much higher background noise relative to the previously done point and area source tests. The thick portion of the water jug is somewhat distinguishable, and its shape is clearer when the reconstruction is superimposed on an actual picture of the experimental setup as shown in Figure 23.



*Figure 23. Water jug reconstruction superimposed on the experimental setup.*

In addition to the issue of background noise, there were a few other reasons why the image was not as clear as in the radioisotope tests. First of all, the x-ray cone-beam could have been reflecting off the steel and concrete back wall because with only 0.25 cm of steel, there was not enough background absorption. A slight shadow of the cone-beam around the target greatly distorts the contours of the image. As described in part 2.2.2, increasing the thickness of steel in the background would help with this noise reduction. Furthermore, for this particular measurement, it was suspected that the detector mask was slightly off-center in relation to the center of the Anger camera, which would explain why the scattering shown in the reconstruction image is also off-center.



### 3.2.2 New Geometry, Water Jug Target

Following the initial water jug acquisitions, the water jug target was retested using the new geometry setup that was optimized to reduce air scatter and noise from environmental sources. The z-distances selected for this set of measurements shown in Table 6 were meant to be similar to the target-detector distance used in the water jug test for the original geometry.

X-ray voltage	225 kVp	
X-ray current	13.3 mA	
Energy window	85 – 140 keV	
Background count rate	~900 cps	
Total counts	1000k	
Acquisition	Distance (cm)	Count rate (cps)
Water jug	518.5	2800
Water jug	515.7	2800
Water jug	508.7	2700
Water jug	500.4	2700
Water jug	492.8	2600
Water jug	484.6	2600
Water jug	477.0	2500

*Table 6. Specifications and count rates for the water jug target at different distances.*

Unexpectedly, the count rate for this test decreases as the distance decreases. This is rather counter-intuitive because one would expect that the count rate would increase as the target becomes larger within the x-ray cone-beam, producing a larger number of scattered events that can still reach the mask. However, the decreasing count rate reveals a problem with the new geometry- that the larger distance between the x-ray tube and the steel background might produce smaller cone-beam than anticipated. In which case, as the target comes closer towards the detector and source, the object actually exits the cone-beam, reducing the number of scatter events.

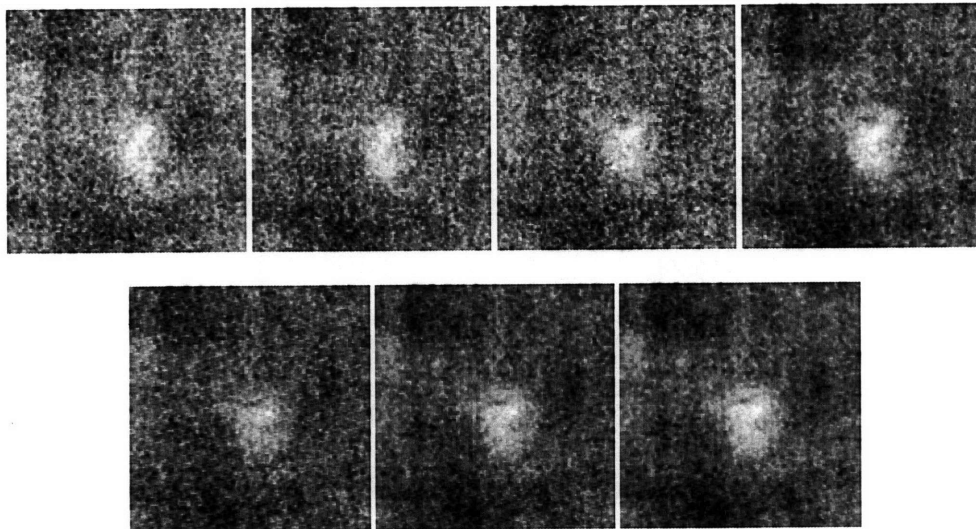


*Figure 24. Reconstructed images of the water jug target at distances between 518.5 and 477.0 centimeters.*

In the reconstructed images of the seven acquisitions, the target is not very distinguishable from the background noise. Although the contours of the top of the water jug become clearer at the closer distances, it is ambiguous whether the bright spot at the center of the images is produced more from scattering off of the target itself or still the steel and concrete background.

### 3.2.3 New Geometry, Arrow Target

The arrow target consists of four inch-thick sheets of polyethylene bonded together. One would expect that this target would produce a large amount of scatter due to its high density of hydrogen, and its sharper edges as well as its consistent thickness would be easier to distinguish in reconstructed images than the rounded curves of the water jug target.

Prior to conducting this experiment, the area of the x-ray cone-beam was checked using a Geiger-Muller counter in order to ensure that most of the target would stay in the cone-beam even as the target moved forward. Initial count rates of the x-ray backscattering were checked with the arrow at different positions to find its optimal position that produced the highest count rate. Then, acquisitions were made with the target-detector distance decreased by approximately seven centimeters per acquisition.

Arrow specifications:

- Thickness: 4 inches
- Base width: 6 inches
- Height: 15 inches

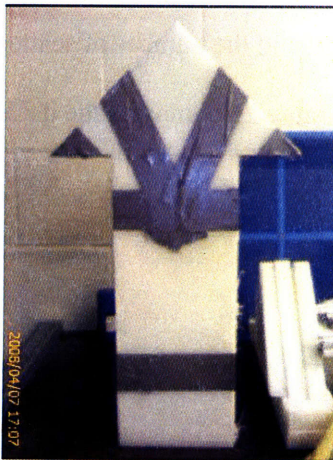


*Figure 25. Four inch thick polyethylene arrow target*

X-ray voltage	225 kVp	
X-ray current	13.3 mA	
Energy window	85 – 140 keV	
Background count rate	~900 cps	
Total counts	1000k	
Acquisition	Distance (cm)	Count rate (cps)
Arrow	523.0	2550
Arrow	516.3	2650
Arrow	509.6	2750
Arrow	502.9	2800
Arrow	496.2	2750

*Table 7. Specifications and count rates for the arrow target at different distances.*

Unlike the water jug test for the new geometry, this measurement showed an increase in the count rate as the distance was reduced, suggesting that the arrow stayed more within the x-ray cone-beam and the number of scatter events increased as the arrow moved closer to the detector. Figure 26 compares the differing trends of the count rates for both targets as the distance decreases.

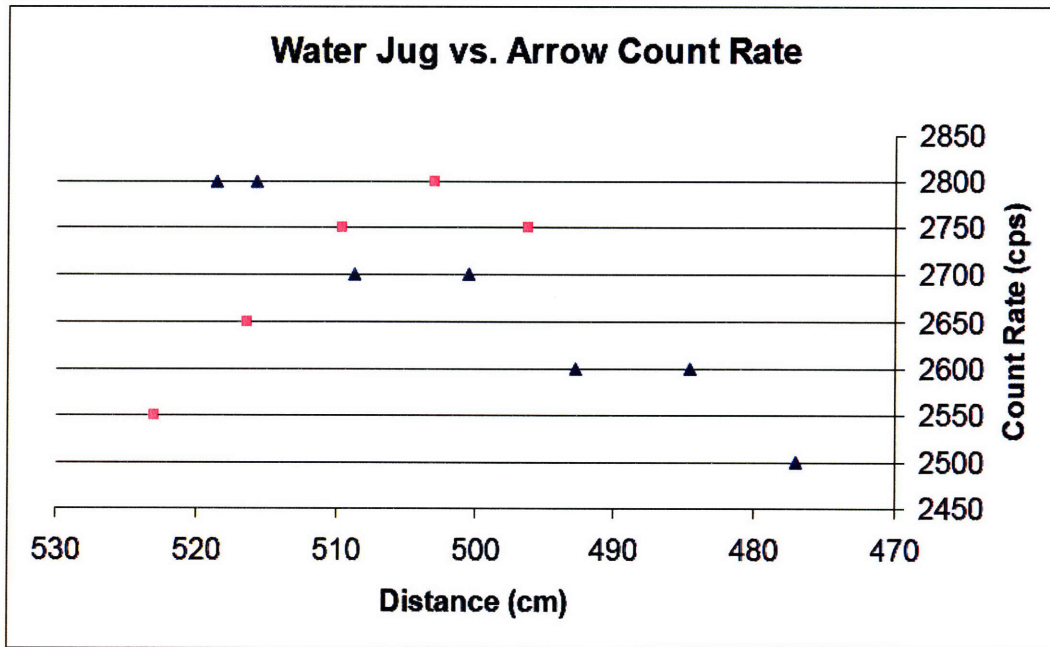


Figure 26. The water jug count rate (triangular series) decreased as distance decreased, however the arrow count rate (square series) increased as distance decreased, due to the movement of the target within the x-ray cone-beam.

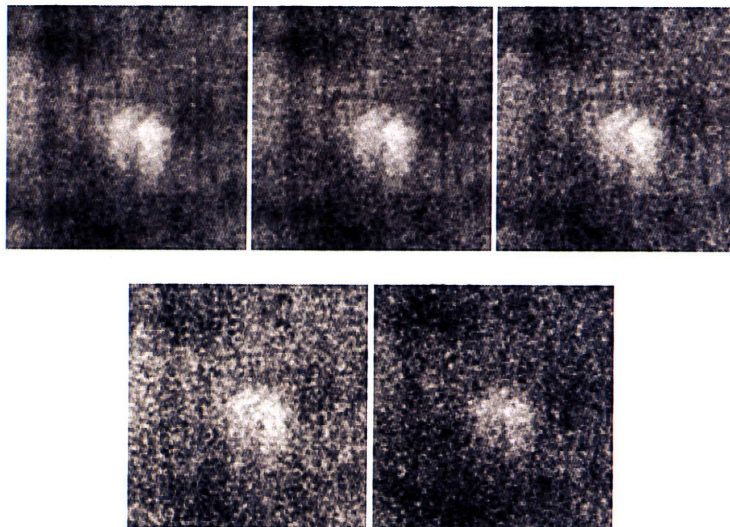


Figure 27. Reconstructed images of the arrow target for five acquisitions for distances between 523.0 and 496.2 centimeters.

The sequence of arrow acquisitions show improved contrast compared to the water jug tests for the initial frames. However, the image quality degrades as target

moves closer to the detector. Although the edges of the top triangular portion of the arrow can be seen in the first two acquisitions, there also appears to be a significant amount of scatter to the left of the arrow, most likely produced by x-ray scattering off the steel background.

## **4. Conclusion**

For this study, a laboratory setup simulated a low Z target moving towards a coded aperture and detector such that dynamic reconstruction algorithms for the coded aperture could be tested. Initial tests showed that for radioisotopic sources with a large number of photon emissions, the x-ray imaging system could clearly resolve the targets. The reconstruction algorithms were successful and produced images with high resolution and low background noise. A subsequent test using a water jug target that produced a much lower resolution image prompted a change in the geometry of the experimental setup. This change involved an increase of the distance between the detector and the target due to presence of radioisotopes in the laboratory that could create additional noise, a slight decrease of the distance between the x-ray source and the target in order to increase the amount of x-ray signal reaching the target, and the addition of a lead shield between the x-ray and detector to reduce high energy air scatter near the detector mask. With this new geometry, a retest of the water jug target still had a relatively low contrast compared with the radioisotope tests and was not very distinguishable. A final test with the new geometry was conducted using a polyethylene arrow target resulted in a clearer image than that of the water jug, but still was not nearly as unambiguous as the Cobalt sources.

The clear images of the Co-60 point source and Co-57 area source even at differing distances between the mask and detector prove the success of the dynamic reconstruction algorithms in interpreting photon signals from changing distances and angles. The coded aperture technique with a unique mask design is able to resolve images even from the relatively low number of counts from x-ray backscattering.

Although the radioisotopic tests prove the principle of the reconstruction algorithms, there are still a number of improvements that could be made to improve image quality for this experiment. First of all, preliminary tests finding the pulse height spectra seen by the detector with the 225 kVp x-ray on and off reveal that the energy window for the camera used during measurements could be narrowed in order to reduce the amount of extra noise entering the camera. Also, increasing the amount of steel behind the target above 0.25 cm helps to absorb photons behind the target and also reduce background noise. Narrowing the energy window could help reduce noise that enters the detector, stemming from background sources (including the radioactive sources present in the laboratory) and air scatter.

One particularly evident change due to the new geometry of the experimental setup was the change in the orientation of the x-ray cone-beam. The steady decrease of the count rate for the water jug retest showed that it was exiting the cone-beam as it moved closer to the detector. The area of this beam would have to be checked prior to the beginning of any experiment to ensure that the target at its initial and final position would stay within the beam.

Overall, this investigation shows very promising results for the end goal of designing an x-ray backscatter imaging system using a coded aperture and capable of detecting low atomic number materials such as a roadside bomb attached to a steel guardrail. The long range x-ray imaging system used in conjunction with coded aperture techniques proved through radioisotope and backscatter target tests that the dynamic reconstruction algorithms are capable of resolving shapes with high photon count rates at varying distances.



## Appendix A: Background Isotopes

Detector #1	ACQ 09-Apr-2008 at 17:02:46 RT = 471.0 LT = 470.3 SCANNERTHING MCB 25 No sample description was entered
ROI # 1	RANGE: 58 = 51.44keV to 68 = 60.34keV AREA : Gross = 702 Net = 117 +/- 24 CENTROID: 63.47 = 56.31keV SHAPE: FWHM = 1.84 FW(1/5)M = 3.71 ID: Hf-181 at 55.79keV Corrected Rate = 1.51 +/- 0.31 cA
ROI # 2	RANGE: 261 = 232.17keV to 275 = 244.63keV AREA : Gross = 1580 Net = 360 +/- 46 CENTROID: 267.94 = 238.35keV SHAPE: FWHM = 2.78 FW(1/5)M = 7.87 ID: Ba-131 at 239.63keV Corrected Rate = 31.79 +/- 4.06 cA
ROI # 3	RANGE: 388 = 345.23keV to 404 = 359.48keV AREA : Gross = 810 Net = 172 +/- 36 CENTROID: 395.11 = 351.57keV SHAPE: FWHM = 3.58 FW(1/5)M = 4.87 ID: Pb-214 at 351.99keV Corrected Rate = 0.99 +/- 0.21 cA
ROI # 4	RANGE: 644 = 573.15keV to 666 = 592.74keV AREA : Gross = 461 Net = 85 +/- 33 CENTROID: 655.53 = 583.42keV SHAPE: FWHM = 3.97 FW(1/5)M = 5.35 ID: Ba-131 at 585.02keV Corrected Rate = 14.65 +/- 5.69 cA
ROI # 5	RANGE: 673 = 598.97keV to 695 = 618.55keV AREA : Gross = 452 Net = 172 +/- 31 CENTROID: 683.78 = 608.56keV SHAPE: FWHM = 2.06 FW(1/5)M = 4.76 ID: Xe-135 at 608.18keV Corrected Rate = 12.58 +/- 2.27 cA

Table 8. Major isotopes found in the pulse height spectra of the background, no x-rays.

## 5. References

1. “The single most effective weapon against our deployed forces” *The Washington Post* <http://www.washingtonpost.com/wp-dyn/content/article/2007/09/29/AR2007092900750.html>
2. Yinon, Jehuda. “Field Detection and Monitoring of Explosives”. *TrAC Trends in Analytical Chemistry, Volume 21, Issue 4, April 2002, Pages 292-301.*
3. Hussein, Esam. “Detection of explosive materials using nuclear radiation: a critical review”. *X-Ray Detector Physics and Applications, Volume 1736, February 1993, Pages 130-137.*
4. Robert J. Leclair and Paul C. Johns. “A semianalytic model to investigate the potential applications of x-ray scatter imaging”. *Medical Physics, Volume 25, Issue 6, June 1998, Pages 1008-1020.*
5. Sunwoo Yuk, Kwang Hyun Kim and Yun Yi “Detection of buried landmine with X-ray backscatter technique”. *Nuclear Instruments and Methods in Physics Research Section A: Accelerators, Spectrometers, Detectors and Associated Equipment, Volume 568, Issue 1, 30 November 2006, Pages 388-392.*
6. F. Cusanno et al. “High-resolution, high sensitivity detectors for molecular imaging with radionuclides: The coded aperture option”. *Nuclear Instruments and Methods in Physics Research Section A: Accelerators, Spectrometers, Detectors and Associated Equipment, Volume 569, November 2006, Pages 193-196.*
7. “Coded Aperture Imaging” <http://www.paulcarlisle.net/old/codedaperture.html>
8. T. Gozani et al. “Gamma ray spectroscopy features for detection of small explosives”. *Nuclear Instruments and Methods in Physics Research Section A: Accelerators, Spectrometers, Detectors and Associated Equipment, Volume 505, November 2003, Pages 482-485.*
9. Byard, Kevin. “An optimized coded aperture imaging system”. *Nuclear Instruments and Methods in Physics Research Section A: Accelerators, Spectrometers, Detectors and Associated Equipment, Volume 313, November 1992, Pages 283-289.*
10. Jean in ‘t Zand. “Coded aperture imaging concept” [http://astrophysics.gsfc.nasa.gov/cai/coded\\_intr.html](http://astrophysics.gsfc.nasa.gov/cai/coded_intr.html)